ORIGINAL PAPER

H. Yang · R.M. Hazen · R.T. Downs · L.W. Finger

Structural change associated with the incommensurate-normal phase transition in akermanite, $Ca_2MgSi_2O_7$, at high pressure

Abstract The structural changes associated with the incommensurate (IC)-normal (N) phase transition in akermanite have been studied with high-pressure single-crystal X-ray diffraction up to 3.79 GPa. The IC phase, stable at room pressure, transforms to the N phase at ~ 1.33 GPa. The structural transformation is marked by a small but discernable change in the slopes of all unit-cell parameters as a function of pressure. It is reversible with an apparent hysteresis and is classified as a tricritical phase transition. The linear compressibility of the a and c axes are 0.00280(10) and 0.00418(6) GPa^{-1} for the IC phase, and 0.00299(11) and 0.00367(8) GPa^{-1} for the N phase, respectively. Weighted volume and pressure data, fitted to a second-order Birch-Murnaghan equation of state ($K'=4.0$), yield $V_0=307.4(1)$ $Å^3$ and $K_0=100(3)$ GPa for the IC phase and $V_0=307.6(2)$ $Å^3$ and $K_0=90(2)$ GPa for the N phase. No significant discontinuities in $Si-O$, $Mg-O$ and $Ca-O$ distances were observed across the transition, except for the $Ca-O1$ distance, which is more compressible in the IC phase than in the N phase. From room pressure to 3.79 GP the volume of the $[SiO_4]$ tetrahedron is unchanged (2.16 $Å^3$), whereas the volumes of the $[MgO_4]$ and $[CaO_8]$ polyhedra decrease from 3.61 to 3.55(1) $Å^3$ and 32.8 to 30.9(2) $Å^3$, respectively. Intensities of satellite reflections are found to vary linearly with the isotropic displacement parametr of Ca and the librational amplitude of the $[SiO_4]$ tetrahedron. At room pressure, there is a mismatch between the size of the Ca cations and the configuration of tetrahedral sheets, which appears to be responsible for the formation of the modulated structure; as pressure increases, the misfit is diminished through the relative rotation and distortion of $[MgO_4]$ and $[SiO_4]$ tetrahedra and the differential compression of individual $Ca-O$ distances, concurrent with a displacement of Ca along the (110) mirror plane toward the O1 atom. We regard the high-pressure normal structure as a result of the elimination of microdomains in the modulated structure.

Introduction

Akermanite, $Ca_2MgSi_2O_7$, is an endmember of the melilite group of minerals and usually occurs in igneous and metamorphic rocks, meteorites, and blast furnace slags. Hemingway et al. (1986) and Seifert et al. (1987) recognized that akermanite and iron-akermanite, $Ca_2(Fe, Mg)Si_2O_7$, exhibit an incommensurate (IC) structure at room temperature with modulations along [110] and [1$\bar{1}$0] and that they undergo a reversible phase transition to a high-temperature normal (N) structure at ca. 353 to 523 K, depending on the composition. Since these studies, the incommensurately-modulated structure has also been observed in many other melilites of different compositions (e.g., Röthisberger et al. 1990; Iishi et al. 1989, 1990, 1991). Because the modulated structure in akermanite is only two-dimensional and stable over a wide range of temperature, it has been the subject of a variety of experimental studies to understand the physical and chemical properties associated with displacively-modulated phases, which include differential scanning calorimetry (Hemingway et al. 1986), adiabatic calorimetry (Iishi et al. 1991; Mizota and Iishi 1994), X-ray, electron, and neutron diffraction (Hemingway et al. 1986; Seifert et al. 1987; Röthlisberger 1989; Iishi et al. 1989; Swainson et al. 1992), optical diffraction (Iishi et al. 1994), transmission electron microscopy (TEM) (Seifert et al. 1987; Röthlisberger 1989; Iishi et al. 1989), differential thermal analysis (Seifert et al. 1987; Röthlisberger 1989), dilatometry (Webb et al. 1992), ^{29}Si nuclear magnetic resonance (NMR) (Merwin et al. 1989), ultrasonic wave propagation (Li et al. 1990), Raman spectroscopy (Sharma et al. 1988), dielectric constant measurements (Shannon et al. 1992) and EXAFS analyses (Tamura et al. 1996). A review of the

Hexiong Yang (✉) · Robert M. Hazen · Robert T. Downs
Larry W. Finger
Geophysical Laboratory, 5251 Broad Branch Road, NW,
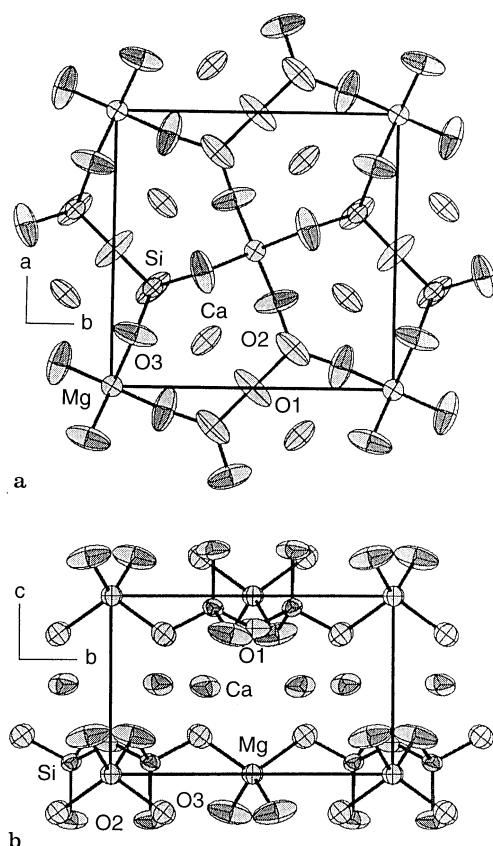Washington, DC 20015-1305, USA

Fig. 1 a, b Crystal structure of akermanite at room pressure: **a** viewed along [001] and **b** viewed along [100]. Atomic displacement ellipsoids are drawn at the 99% probability density level

macroscopic and microscopic changes at the IC-N phase transition in melilites has been given by Seifert and Röthlisberger (1993). In general, an incommensurately-modulated phase may be regarded as an intermediate state between an unmodulated structure (in this case, the normal akermanite structure) and a commensurate superstructure (so-called "lock-in phase") (e.g., Salje 1990). Although the modulation wavelength in akermanite has been found to vary with temperature (Seifert et al. 1987), no experiment has discovered the existence of a low-temperature superstructure down to 77 K (Röthlisberger 1989). In fact, no low-temperature superstructure has been reported as yet for any of the melilite group of minerals.

The crystal structures of both the IC and N phases of akermanite are tetragonal and have been described as the same space group $P\bar{4}2_1m$. They can be characterized by tetrahedral sheets consisting of $[Si_2O_7]$ dimers interconnected by tetrahedrally coordinated Mg cations in the form of five-membered rings. These sheets lie parallel to the (001) plane and are linked together along c by large Ca cations in distorted eight-coordinated sites (Fig. 1). Kimata and Ii (1981) refined the structure of a synthetic akermanite crystal at ambient conditions, but their Weissenberg photographs, possibly due to the short exposure time, did not reveal the presence of superstructure reflec-

tions. Using Mössbauer spectroscopy Seifert et al. (1987) found that there exist two distinct $[(Fe, Mg)O_4]$ tetrahedral sites in modulated Fe-akermanites and that the two sites become less distinguishable as temperature approaches the phase transition critical temperature and merge into one site in the normal structure. The ^{29}Si MAS NMR spectra measured by Merwin et al. (1989) demonstrate the existence of three or more nonequivalent Si sites in incommensurately-modulated akermanite. Based on the structural refinement of a $Ca_2ZnGe_2O_7$ melilite that possesses an IC structure at room temperature, Armbruster et al. (1990) noticed the strong anisotropy of several atomic displacement ellipsoids and suggested the linkage between modulation and the librations of tetrahedral units about an axis parallel to c. Hagiya et al. (1993) performed a five-dimensional refinement of the modulated structure of Co-akermanite $(Ca_2CoSi_2O_7)$ and concluded that the modulation is caused by static displacements of the constituent atoms from their dynamically-averaged positions. Despite intensive studies on the incommensurability in akermanite, structural details on the IC-N phase transition are still unclear because of the lack of data at the atomic level. This paper reports the results of a systematic structural study of akermanite carried out at pressures below and above the IC-N transition in order to shed light on the atomic level structural changes associated with the phase transformation.

Experimental procedures

Room-pressure X-ray diffraction data measurements

Following the procedure described by Hemingway et al. (1986) for their AK1 sample synthesis, the akermanite sample used in this study was synthesized by melting a stoichiometric mixture of Ca-CO_3, MgO, and SiO_2 compounds at 1500 °C for 2 hours and slowly cooling to 800 °C for 48 hours. The crystal was chosen on the basis of optical examination and precession photographs. Incidentally, in the course of selecting a suitable single crystal for the high-pressure experiment, we found that significant broadening of diffraction profiles resulted when an otherwise good crystal of akermanite was subjected to minimal mechanical force at room temperature, such as produced by slightly cutting or polishing. We also observed the same deterioration of peak profile quality in other samples provided by G.L. Nord (studied by Hemingway et al. 1986), H.S. Yoder (synthesized hydrothermally), and K. Iishi (synthesized by floating-zone method). By trying different methods, we found that crystals crushed in liquid nitrogen show sharpest peak profiles and minimum diffuse background; a single crystal fragment ($0.11 \times 0.10 \times 0.05$ mm in size) was thus selected for the high-pressure study. To ensure the existence of the modulated structure in the selected crystal, a long exposure (001) precession photograph was taken, which displays a complex set of satellite reflections similar to those observed by Hemingway et al. (1986) and Seifert et al. (1987). A Picker four-circle diffractometer equipped with a Mo X-ray tube (β-filtered) was used for all X-ray measurements. Unit-cell parameters, determined by fitting the positions of 18 reflections from the average structure with $20° < 2\theta < 35°$ following the procedure of King and Finger (1979), are $a=7.8349(4)$, $c=5.0079(4)$ Å, and $V=307.41(4)$ Å^3. These values agree with those determined by Kimata and Ii on a synthetic akermanite crystal (1981) [$a=7.835(1)$, $c=5.010(1)$ Å, and $V=307.5(1)$ Å^3]. Positions and intensities of two strong satellite

Table 1 Crystal data and other relevant information on akermanite at various pressures

P(GPa)	a(Å)	c(Å)	V(Å³)	c/a	total refls.	Refls. >3σ(I)	R(int.)	Rw	R
0.00*	7.8338(6)	5.0082(5)	307.35(5)	0.6393	620	210	0.022	0.049	0.041
0.39	7.8261(7)	5.007(6)	306.28(6)	0.6390					
0.80*	7.8154(4)	4.9919(4)	304.91(3)	0.6387	618	207	0.023	0.042	0.034
0.94§	7.8129(5)	4.9889(4)	304.53(4)	0.6385					
1.25*	7.8071(5)	4.9821(4)	303.66(4)	0.6381	615	209	0.023	0.048	0.040
1.37*	7.8046(5)	4.9772(4)	303.17(4)	0.6377	616	215	0.024	0.043	0.035
1.80*	7.7937(5)	4.9696(4)	301.86(4)	0.6376	608	211	0.023	0.049	0.041
2.27	7.7792(6)	4.9587(5)	300.08(5)	0.6374					
2.78*	7.7677(5)	4.9495(4)	298.64(4)	0.6372	605	206	0.022	0.044	0.035
3.29	7.7574(4)	4.9413(3)	297.36(3)	0.6370					
3.79*	7.7494(5)	4.9328(4)	296.23(4)	0.6365	589	212	0.025	0.051	0.044
4.28	7.7341(5)	4.9215(4)	294.39(4)	0.6363					

*: X-ray intensity data were collected at these pressures
§: Data were obtained on decreasing pressure

Table 2 Atomic positional and displacement parameters ($\times 10^4$) of akermanite at various pressures

P(GPa)		0.00	0.80	1.25	1.37	1.80	2.78	3.79
Ca	x	3324(2)	3327(1)	3329(2)	3329(1)	3331(1)	3336(1)	3340(2)
	z	5065(5)	5063(4)	5065(5)	5056(4)	5053(4)	5050(4)	5050(5)
	β_{11}	81(2)	68(2)	57(2)	56(2)	55(2)	48(2)	42(2)
	β_{33}	141(9)	127(8)	127(9)	137(7)	110(9)	113(8)	112(9)
	β_{12}	49(2)	35(2)	25(2)	24(2)	21(2)	17(2)	16(2)
	β_{13}	8(3)	9(2)	5(3)	5(2)	10(3)	7(2)	6(3)
	Biso	1.80(7)	1.53(6)	1.34(6)	1.37(5)	1.26(5)	1.15(5)	1.04(5)
Mg	β_{11}	37(4)	27(3)	22(3)	27(3)	24(3)	20(3)	19(4)
	β_{33}	200(21)	157(17)	166(20)	165(16)	136(19)	147(17)	138(21)
	Biso	1.27(9)	0.95(9)	0.90(9)	0.98(8)	0.83(9)	0.81(8)	0.76(9)
Si	x	1396(2)	1398(2)	1398(2)	1403(2)	1404(2)	1405(2)	1406(2)
	z	9358(5)	9354(4)	9354(5)	9343(4)	9346(5)	9348(5)	93544(5)
	β_{11}	32(3)	32(2)	32(2)	34(2)	32(2)	29(2)	26(3)
	β_{33}	122(12)	82(10)	57(11)	62(9)	80(13)	61(10)	38(12)
	β_{12}	5(3)	5(3)	9(3)	6(3)	− 1(3)	3(3)	5(3)
	β_{13}	6(3)	5(2)	2(3)	3(2)	− 1(3)	− 1(3)	− 2(3)
	Biso	0.93(7)	0.79(7)	0.71(6)	0.75(6)	0.78(6)	0.66(5)	0.53(6)
O1	z	1799(239	1827(19)	1857(22)	1839(20)	1838(23)	1837(19)	1835(23)
	β_{11}	104(11)	96(10)	70(10)	62(8)	72(10)	77(10)	62(11)
	β_{33}	130(53)	60(45)	86(49)	156(46)	92(50)	50(43)	74(53)
	β_{12}	− 72(15)	− 33(15)	− 34(15)	− 49(13)	− 42(15)	− 46(14)	− 29(15)
	Biso	2.1(3)	1.8(3)	1.4(2)	1.5(2)	1.5(2)	1.4(2)	1.2(2)
O2	x	1407(6)	1403(6)	1402(6)	1404(5)	1404(6)	1399(6)	1396(6)
	z	2529(17)	2561(14)	2570(17)	2551(14)	2558(16)	2844(14)	2601(18)
	β_{11}	90(8)	81(8)	60(8)	69(7)	59(7)	58(7)	50(8)
	β_{33}	197(40)	136(30)	206(36)	184(30)	152(34)	168(31)	217(40)
	β_{12}	54(11)	22(11)	25(11)	20(10)	21(11)	5(10)	15(11)
	β_{13}	− 11(12)	− 14(9)	− 18(11)	− 12(9)	− 13(10)	− 23(10)	− 17(12)
	Biso	2.1(2)	1.8(2)	1.7(2)	1.7(2)	1.5(2)	1.5(1)	1.5(2)
O3	x	798(7)	813(7)	814(7)	813(6)	813(6)	820(6)	822(7)
	y	1862(6)	1852(6)	1849(6)	1857(5)	1853(6)	1848(6)	1839(6)
	z	7856(11)	7834(11)	7828(13)	7841(10)	7819(12)	7799(11)	7783(12)
	β_{11}	152(9)	114(9)	90(9)	93(7)	81(8)	70(7)	62(8)
	β_{22}	57(7)	59(7)	38(7)	25(6)	32(7)	35(6)	22(7)
	β_{33}	164(26)	111(21)	164(27)	136(20)	105(21)	127(20)	134(25)
	β_{12}	− 12(8)	− 21(8)	− 7(8)	− 6(6)	− 12(7)	− 8(7)	− 7(7)
	β_{13}	32(12)	37(10)	40(12)	30(10)	24(11)	27(10)	21(11)
	β_{23}	− 14(11)	− 10(10)	− 2(11)	− 4(9)	− 22(10)	− 19(10)	− 16(11)
	Biso	2.3(2)	1.8(1)	1.6(1)	1.4(1)	1.3(1)	1.3(1)	1.1(1)

Note: The following constraints apply to some atomic positional parameters: y=0.5−x for Ca, Si, and O2; x=y=z=0 for Mg; x=0.5, y=0 for O1.

The following constraints apply to some atomic anisotropic displacement parameters: $\beta_{22}=\beta_{11}$ for Ca, Mg, Si, O1, and O2; $\beta_{23}=\beta_{13}$ for Ca, Si, and O2; $\beta_{12}=\beta_{13}=\beta_{23}=0$ for Mg; $\beta_{13}=\beta_{23}=0$ for O1

Table 3 Selected bond distances (Å) in akermanite at various pressures

P (GPa)	0.00	0.80	1.25	1.37	1.80	2.78	3.79
Ca–O1	2.475(8)	2.455(6)	2.438(7)	2.442(7)	2.437(7)	2.423(6)	2.413(8)
Ca–O2	2.475(6)	2.466(5)	2.462(5)	2.464(4)	2.459(5)	2.453(5)	2.449(5)
Ca–O2' [×2]	2.707(5)	2.689(4)	2.683(4)	2.687(4)	2.681(4)	2.660(4)	2.644(5)
Ca–O3 [×2]	2.427(6)	2.407(6)	2.405(6)	2.408(5)	2.400(6)	2.386(5)	2.376(6)
Ca–O3' [×2]	2.685(6)	2.682(6)	2.676(6)	2.675(5)	2.666(6)	2.654(5)	2.647(6)
Mg–O3 [×4]	1.916(5)	1.915(5)	1.913(5)	1.913(4)	1.914(5)	1.911(5)	1.906(5)
Si–O1	1.652(4)	1.654(4)	1.657(4)	1.657(4)	1.656(4)	1.651(4)	1.649(4)
Si–O2	1.588(9)	1.601(7)	1.602(8)	1.597(7)	1.596(8)	1.602(7)	1.602(9)
Si–O3 [×2]	1.627(5)	1.630(5)	1.631(5)	1.617(4)	1.623(5)	1.624(5)	1.629(5)

Table 4 Selected interatomic angles (°) and cation polyhedral parameters in akermanite at various pressures

P (GPa)	0.00	0.80	1.25	1.37	1.80	2.78	3.79
O3–Mg–O3' [×4]	108.3(2)	108.6(2)	108.7(2)	108.4(1)	108.7(2)	109.0(2)	109.2(2)
O3–Mg–O3'' [×2]	111.8(3)	111.3(3)	111.1(4)	111.6(3)	111.0(3)	110.5(3)	110.0(3)
O1–Si–O2	111.0(4)	111.1(3)	111.5(4)	110.8(4)	110.8(4)	110.6(3)	110.5(4)
O1–Si–O3 [×2]	101.2(3)	101.7(3)	101.5(3)	101.7(3)	101.5(3)	101.5(3)	101.5(3)
O2–Si–O3 [×2]	117.3(2)	117.7(2)	117.7(2)	117.5(2)	117.9(2)	118.3(2)	118.6(2)
O3–Si–O3'	105.0(4)	104.7(4)	104.6(4)	105.3(4)	104.9(4)	104.2(4)	103.7(4)
Si–O1–Si'	138.9(8)	138.2(6)	137.3(7)	138.4(7)	138.4(8)	138.4(6)	138.3(8)
O2–O1–O2'	71.4(4)	70.6(3)	70.1(4)	70.7(3)	70.6(4)	70.2(3)	69.9(4)
O3–O1–O3'	118.1(3)	118.5(3)	118.6(3)	118.6(2)	118.5(3)	118.7(2)	118.6(3)
Si–O3–Mg	118.3(3)	117.7(3)	117.6(4)	118.1(3)	117.4(3)	116.9(3)	116.4(3)
[SiO₄] V (Å³)	2.16(1)	2.18(1)	2.18(1)	2.15(1)	2.16(1)	2.16(1)	2.16(1)
QE*	1.012(5)	1.012(5)	1.013(6)	1.012(5)	1.013(6)	1.014(5)	1.015(6)
AV**	52(1)	56(1)	58(1)	54(1)	58(1)	62(1)	65(1)
[MgO₄] V (Å³)	3.61(1)	3.60(1)	3.59(2)	3.59(1)	3.59(1)	3.58(1)	3.55(1)
QE	1.001(1)	1.000(1)	1.000(1)	1.001(1)	1.000(1)	1.000(1)	1.000(1)
AV	3.6(2)	2.1(2)	1.8(2)	3.0(2)	1.6(2)	0.9(1)	0.4(1)
[CaO₈] V (Å³)	32.84	32.25	32.00	32.11	31.85	31.28	30.90

* QE – quadratic elongation; ** AV – angle variance (Robinson et al. 1971)

reflections selected from the precession photograph were measured immediately after the unit-cell determination. Indexed based on the unit-cell vectors of the average structure, these two satellite reflections have hkl values of 2.72 4.28 0 and 2.72 7.72 0, respectively, and their corresponding modulation wavevectors are $\mathbf{k}_1 = 0.28(-\mathbf{a}+\mathbf{b})$ and $\mathbf{k}_2 = 0.28(-\mathbf{a}-\mathbf{b})$, respectively.

X-ray intensity data from one octant of reciprocal space with $0° \leq 2\theta \leq 60°$ were collected using ω scans of 1° width in step increments of 0.025° and 3-s per step counting time. Two standard reflections were checked every 5 hours; no significant or systematic variations in intensities of the standard reflections were observed. Digitized step data were integrated by the method of Lehmann and Larsen (1974) utilizing an option to manually reset backgrounds when necessary. Corrections were made for Lorentz and polarization effects, and for X-ray absorption by the crystal ($\mu = 22.88$ cm^{-1}). The total number of measured reflections was 563. After symmetry equivalent reflections were averaged in Laue group 4/mmm ($R_{int} = 0.013$), there were 284 reflections with I $> 3\sigma(I)$, where $\sigma(I)$ is the standard deviation determined from the counting statistics.

The initial structural model of akermanite was taken from Kimata and Ii (1981). Least-squares refinements were performed using an updated version of RFINE4 (Finger and Prince 1975), in the space group $P\bar{4}2_1m$. Neutral atomic scattering factors, including anomalous dispersion correction for Ca, Mg, Si, and O, were taken from Ibers and Hamilton (1974). Weighting schemes were based on $W = [\sigma^2(F) + (pF)^2]^{-1}$, where p is adjusted to ensure that the errors were normally distributed through probability plot analysis (Ibers and Hamilton 1974). Type II isotropic extinction corrections (Becker and Coppens 1975) were applied in the refinements. Final R_w and R factors are 0.031 and 0.024, respectively. (Atomic positional coordinates and displacement parameters are available from the first author upon request).

High-pressure X-ray diffraction data measurements

After the X-ray intensity data collection at room pressure, the crystal was mounted in a Merrill-Bassett diamond-anvil cell with a mixture of 4:1 methanol:ethanol as the pessure medium. Four small (~10 µm) ruby chips were included as the internal pressure calibrant (Hazen and Finger 1982), from which pressure was determined from the average position of the R_1 laser-induced fluorescence peaks, with an error of approximately 0.05 GPa. The fixed-φ mode of data measurement (Finger and King 1978) was employed throughout the high-pressure experiments to maximize reflection accessibility and minimize attenuation by the diamond cell. Lattice constants were determined using the same method as described for the room-pressure experiment. The two satellite reflections measured after the unit-cell determination at each pressure became undetectable as pressure was increased from 1.25 to 1.37 GPa. After the intensity data collection at 3.78 GPa, the pressure of the crystal was gradually released to check the reversibility of the phase transition; the satellite reflections reappeared between 1.18 and 0.94 GPa. Next, the pressure was raised to 4.57 GPa. Some of the peak profiles of reflections used to determine the unit-cell dimensions became considerably broadened and/or were composed of two or more peaks at this pressure. After the complete release of pressure, the quality of the crystal did not recover.

X-ray intensities of the average structure were collected for all accessible reflections in a hemisphere of reciprocal space with $0° \leq 2\theta \leq 60°$. For better comparison with high-pressure data we collected another set of room-pressure X-ray intensity data while the crystal was mounted in the diamond-anvil cell. The experimental procedures for X-ray data collection, reduction, and structure refinements were similar to those described above for the data collected in air; in addition, corrections were made for absorption by the diamond and beryllium components of the pressure cell. Unit-cell dimensions and final refinement statistics are given in Table 1; atomic positional and displacement parameters are listed in Table 2; selected interatomic distances and angles are presented in Table 3 and 4, respectively.

Results and discussion

Satellite reflections

The modulation wavelength in akermanite and other melilite minerals has been found to increase with increasing temperature (Seifert and Röthlisberger 1993). However, we did not observe significant variation of the modulation wavelength with pressure: it remains ~ 19.78 Å (the d-spacing of the modulation wavevector) between room pressure and 1.25 GPa. This value is comparable with modulation wavelengths of 19.86 Å reported by Seifert et al. (1987) and 19.73 Å by Iishi et al. (1989) for synthetic akermanite. However, satellite intensities, which are proportional to the modulation amplitude, were found to decrease monotonically with increasing pressure with the rate of decrease becoming greater as the IC-N transition pressure was approached (Fig. 2). From 1.25 to 1.37 GPa, the satellite intensities became undistinguishable from the background and remained undetectable at higher pressures. Our observation of the variation of satellite intensities with pressure is similar to that made by Hagiya et al. (1993) on Co-akermanite as a function of temperature using synchrotron radiation. However, Hemingway et al. (1986) and Seifert et al. (1987) found by in-situ TEM measurements that some very diffuse and weak relic intensities of satellite reflections were still visible on overexposed diffractograms above the phase transition temperature. The IC-N transition pressure was determined to be ~ 1.33 GPa by a fit of the data to a Landau free energy expansion, which is considerably lower than that (~ 1.78 GPa) extrapolated from data obtained by Röthlisberger (1989) using high-pressure differential thermal analyses up to 0.5 GPa.

The positions and the peak widths of satellite reflections that reappeared between 1.18 and 0.94 GPa on the release of pressure were essentially unchanged compared to those that were originally measured at increasing pressures. Together with the unit-cell parameters determined at 0.94 GPa, which conform to the trends defined by the unit-cell parameters determined as pressure was raised, the IC-N transition in akermanite was ascertained to be reversible with an apparent hysteresis. The hysteresis effect associated with the IC-N transition in akermanite has also been detected by differential thermal analysis at high temperatures (Seifert et al. 1987)
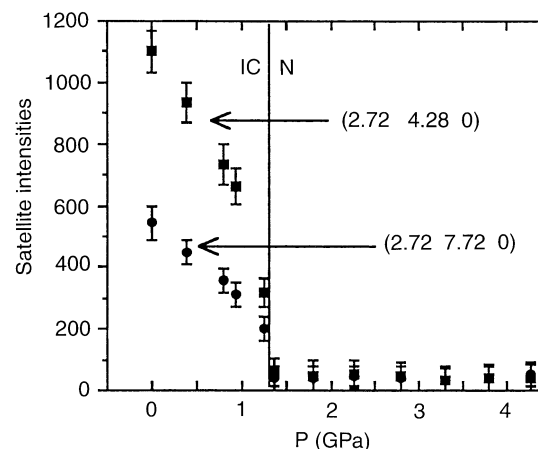

Fig. 2 Pressure dependence of the intensities of satellite reflections (2.72 4.28 0) and (2.72 7.72 0)

and dilatometry (Webb et al. 1992), but not by calorimetric measurements (Hemingway et al. 1986; Mizota and Iishi 1994).

Unit-cell parameters

Variations of unit-cell dimensions with pressure are plotted in Fig. 3. The IC-N transition at ~ 1.31 GPa is marked by a small but discernible change in the slopes for all the plots, showing that the a axis in the N phase is slightly more compressible than in the IC phase, whereas the c axis in the N phase is less compressible than in the IC phase. The linear compressibilities of the a and c axes are $0.00280(10)$ and $0.00418(6)$ GPa^{-1} for the IC phase, respectively, and $0.00292(11)$ and $0.00367(8)$ GPa^{-1} for the N phase, respectively. As a result, there is a noticeable change of slope in the plot of c/a vs. pressure, which is steeper for the IC phase. The axial compression ratios are $a:c=1:1.45$ for the IC phase and $1:1.26$ for the N phase. These results imply a change in the compression mechanism in akermanite at the transition. Note that a sudden change has also been detected in the thermal expansivity of akermanite and Co-akermanite at the transition temperatures, particularly in that of the c dimension (Hemingway et al. 1986; Webb et al. 1992; Brown et al. 1994). Weighted volume and pressure data fit to a second-order Birch-Murnaghan equation of state ($K' \equiv 4.0$) yield $V_0 = 307.4(1)$ Å^3 and $K_0 = 100(3)$ GPa for the IC phase and $V_0 = 307.6(2)$ Å^3 and $K_0 = 90(2)$ GPa for the N phase. The bulk modulus for the IC phase obtained in this study is slightly larger than that (94.4 GPa) determined by Li et al. (1990) using the ultrasonic phase comparison method at ambient conditions.

Structural variations with pressure

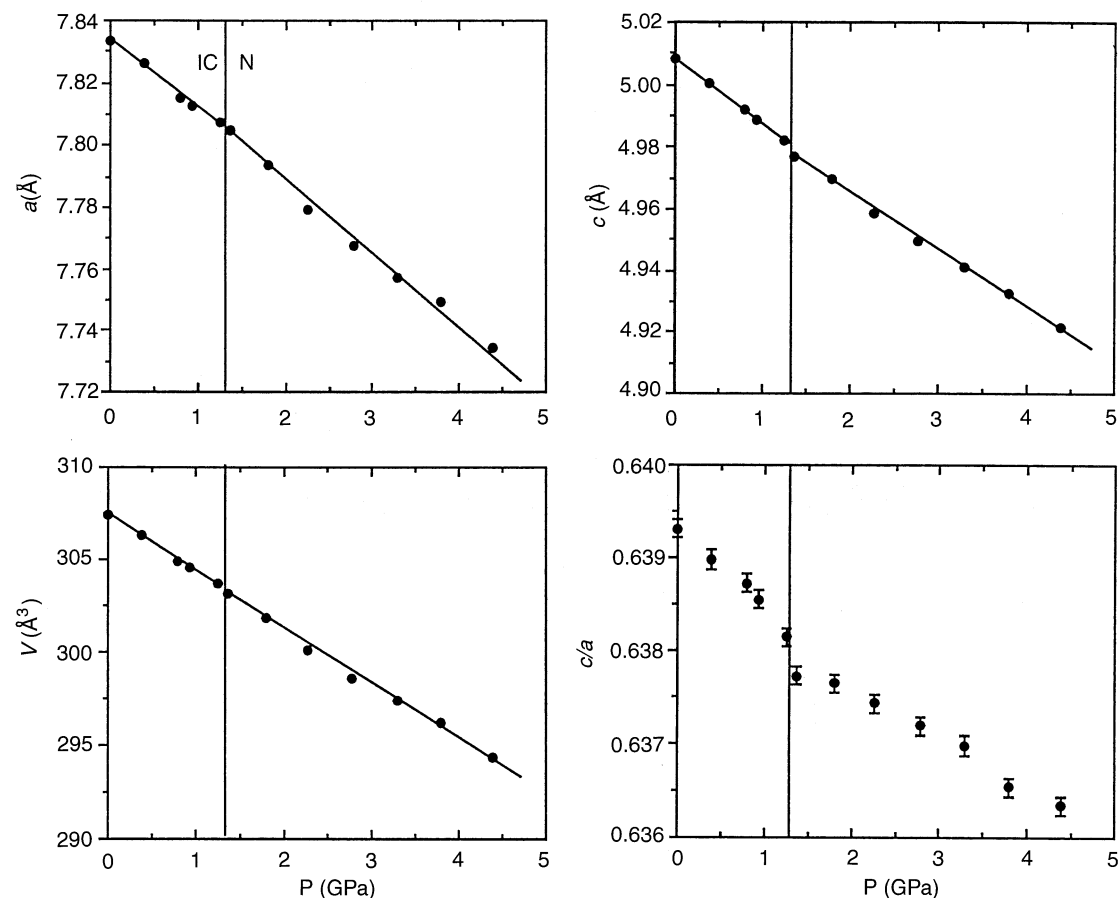At room pressure, atomic displacement ellipsoids for Si and Mg are relatively small and spherical, whereas those

Fig. 3 Variations of unit-cell parameters with pressure

for Ca and O (O 1, O 2, and O 3) are considerably larger and highly anisotropic with the longest axes of the ellipsoids lying approximately in the (001) plane (Fig. 1), demonstrating the strong positional disorder of these atoms in the plane. Similar results were found by Armbruster et al. (1990) from the refinement of the average structure of $Ca_2ZnGe_2O_7$ melilite. Independent evidence for strong positional disorder of Ca has also been obtained by Shannon et al. (1992), who attributed the unusually large dielectric constants of $Ca_2MgSi_2O_7$, $Ca_2CoSi_2O_7$, and $Ca_2ZnSi_2O_7$ melilites to a "rattling" effect of the Ca cation in the structure.

Finger and King (1978) have demonstrated that pressure has a small, but possibly measurable, effect on the atomic isotropic displacement factors (B_{iso}); for NaCl they predicted a $\sim 6\%$ reduction in the B_{iso} factors for Na and Cl from room pressure to 3.2 GPa, which agrees with the measured reduction of $\sim 10\%$ ($\pm 5\%$). However, we observed a more pronounced decrease in all atomic B_{iso} parameters in the IC phase of akermanite. All atomic B_{iso} values decrease by more than 20% between room pressure and 1.25 GPa (Table 2). The anisotropy of atomic displacement ellipsoids for O and Ca also decrease appreciably with increasing pressure, especially for Ca (Fig. 4). The significant decrease in the size and anisotropy of the displacement ellipsoid for Ca indicates a
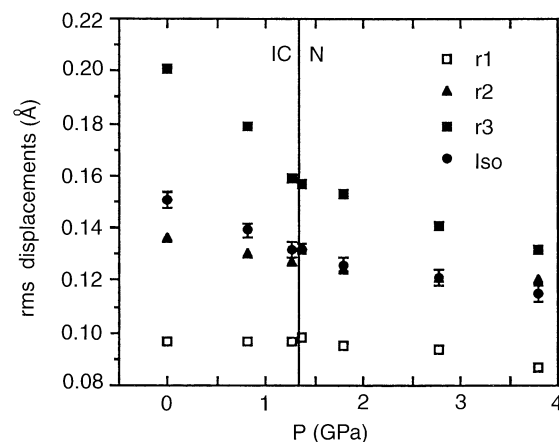

Fig. 4 Root-mean-square displacements (RMS) of Ca as a function of pressure

great decrease in its positional disorder. It also suggests that the large displacement ellipsoid of Ca at ambient conditions likely results principally from atomic static disorder, rather than the large, anisotropic thermal vibrations. Furthermore, pressure appears to have a stronger influence on atomic displacement parameters for the IC structure than for the N structure (Fig. 4).
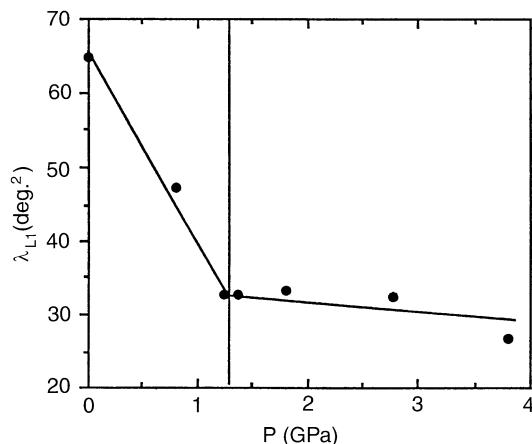
Fig. 5 The largest librational eigenvalue (λ_{L1}) of the [SiO$_4$] tetrahedron as a function of pressure

Fig. 6 The component of the Ca–O1 distance along c as a function of pressure

Analysis of the Raman spectra of akermanite (Sharma et al. 1988) suggests that the vibrational characteristics in the structure are strongly affected by the [Si$_2$O$_7$] silicate group, and not by the sheet-like structure interconnected by [MgO$_4$] tetrahedra, and that the silicate unit acts as a librationally isolated entity. To gain insight into the relationship of the [SiO$_4$] tetrahedral libration with the IC-N transformation, we applied rigid-body thermal vibration analysis to the determined displacement parameters using the program THMA 14 (Trueblood 1978). The results show that (i) the amplitude of the largest libration eigenvalue (λ_{L1}) decreases considerably from room pressure to 1.25 GPa, but remains virtually unchanged for the N phase between 1.37 and 3.79 GPa (Fig. 5), and (ii) the principal libration axis of the [SiO$_4$] group is approximately parallel to **c** throughout the studied pressure range. The librational motion of the [SiO$_4$] group along **c**, which lies on the (001) plane between two [CaO$_8$] polyhedral layers, primarily involves the overbonded, bridging O1 atom and the charge-balanced, bridging O3 atom. Because such a librational motion requires minimal out-of-plane tilting of the [SiO$_4$] tetrahedron and compression of the [CaO$_8$] polyhedral layers, it is energetically the easiest and thus the largest.

No significantly abrupt changes in Si–O and Mg–O bond lengths were observed across the IC-N transition. Within the experimental errors the Si–O bond lengths are constant, whereas the Mg–O distance compresses only by about one standard deviation. In the pressure range of the experiment the rigid behavior of the Si–O bond is expected, considering its bond strength and the flexibility of the structure. Similar results have also been reported for other layer silicate minerals (Hazen and Finger 1978a). Individual O–Si–O angles within the [SiO$_4$] tetrahedron, however, respond to pressure differently: while the O1–Si–O2 and O1–Si–O3 angles remain unchanged up to 3.79 GPa, the O2–Si–O3 angle increases slightly from 117.3°(2) to 118.6°(2) and the O3–Si–O3′ angle decreases from 105.0°(4) to 103.7°(4). As a consequence, the [SiO$_4$] tetrahedron be-

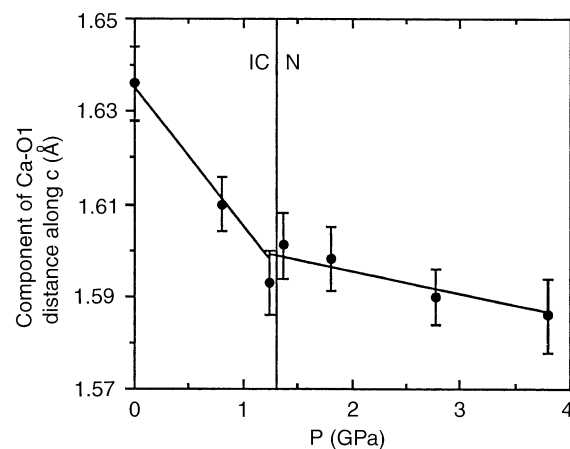comes more distorted at higher pressures, as shown by the tetrahedral angle variance (TAV) (Robinson et al. 1971) (Table 4). In contrast, the [MgO$_4$] tetrahedron becomes more regular at elevated pressures owing to the change in the O3–Mg–O3″ angle and approaches a nearly ideal geometry at 3.79 GPa. Within the experimental uncertainties the volume of the [SiO$_4$] tetrahedron ($\sim$2.16 Å^3) is unaffected by pressure up to 3.79 GPa, whereas that of the [MgO$_4$] tetrahedron decreases from 3.61(1) Å^3 at room pressure to 3.55(1) Å^3 at 3.79 GPa. The calculated linear bulk modulus for the [MgO$_4$] tetrahedron is 250(31) GPa.

At room temperature, Ca in akermanite is eight-coordinated with four closer O atoms (one O1, one O2, and two O3) at a distance of $\sim$2.45 Å and four farther ones (two O2′ and two O3′) at a distance of $\sim$2.70 Å; the mean Ca–O distance of 2.57 Å is considerably larger than the typical Ca–O distance of 2.50 Å calculated from ionic radii (Shannon 1976), as also noted by Kimata and Ohashi (1982). The bond valence calculated for Ca is only 1.662 (Brown 1981), indicating that Ca is substantially underbonded in the structure. With increasing pressure all Ca–O distances decrease nearly linearly, except the Ca–O1 distance, which shows a greater rate of decrease for the IC phase than for the N phase, especially in the plot of its component along c (Fig. 6). Between room pressure and 3.79 GPa the Ca–O1 distance decreases most (2.5%) and the Ca–O2 distance least (1.1%). The largest decrease in the Ca–O1 distance is partially due to the significant displacement of Ca toward O1 along the (110) mirror plane (Table 2). There is a linear relationship between the [CaO$_8$] polyhedral volume and the unit-cell volume (Fig. 7), suggesting that the high-pressure behavior of the [CaO$_8$] polyhedron is a major factor controlling the compression of the akermanite structure. The volume of the [CaO$_8$] polyhedron compresses by as much as 5.9% between room pressure and 3.79 GPa, yielding a bulk modulus of 65(4) GPa. Compared to the bulk moduli determined for the [CaO$_8$] polyhedron in diopside (101 GPa) (Levien and Prewitt 1981),
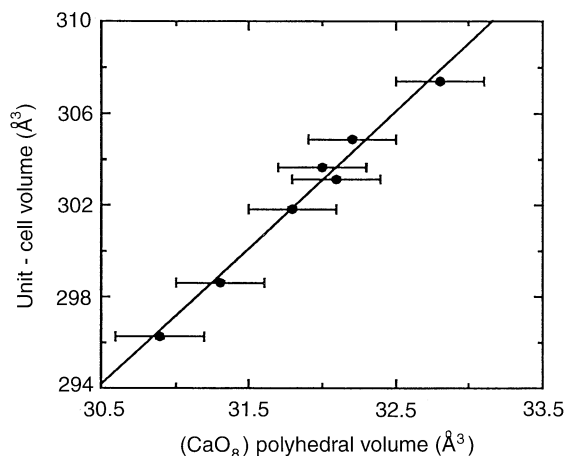
Fig. 7 The unit-cell volume vs. the mean Ca–O distance

Fig. 8 Squared intensities of satellite reflections as a function of pressure

fassaite (90 GPa) (Hazen and Finger 1977), and grossular (115 GPa) (Hazen and Finger 1978b), the bulk modulus of the [CaO$_8$] polyhedron in akermanite is substantially smaller, which can be attributed to the longer mean Ca–O distance in akermanite at room pressure than the typical Ca–O distance.

For layer silicate compounds, such as phlogopite and chlorite, Hazen and Finger (1978a) demonstrated that compression within the layers is restricted by the strength of the polyhedral sheets, whereas that perpendicular to the layers is determined by the interlayer weaker bonds. Similar conclusions can be drawn here. In akermanite, the Si–O and Mg–O bonds are nearly rigid; hence, compression along the a axis is primarily achieved through changes in interatomic angles within the tetrahedral sheets, such as Mg–O3–Si, O3–Si–O3 and O3–Mg–O3, all of which decrease with increasing pressure (Table 4). There is a sudden change in the rate of decrease for some interatomic angles at the transition pressure. For example, the O3–Si–O3 angle decreases at a rate of $-0.33°$/GPa for the IC phase, but at a rate of $-0.66°$/GPa for the N phase. The different behavior of interatomic angles within the tetrahedral sheets below and above the transition could account for the slightly larger compressibility of the a axis in the N phase relative to that in the IC phase. On the other hand, because the relatively compressible [CaO$_8$]-polyhedra are interleaved by more rigid tetrahedral sheets along **c**, the behavior of the Ca–O bonds at high pressure dominates the compressibility of the structure in the c dimension. Accordingly, the c axis always compresses more than the a axis. The less compressible c axis of the N phase compared to that of the IC phase can be explained by the evident change in the compressibility of the Ca–O1 bond along **c**.

Order and mechanism of the IC-N phase transition

The order of the IC-N phase transition in akermanite has been a matter of controversy. On the one hand, calorimetric measurem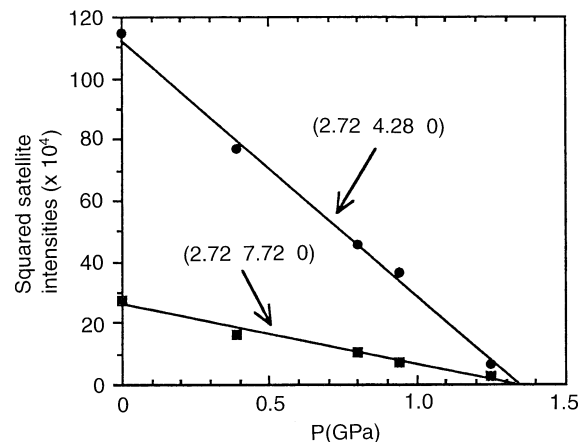ents of Hemingway et al. (1986) show that the transition is characterized by a sharp λ-type peak with no sign of hysteresis, a typical feature of the second-order phase transition. Similar results were obtained by Iishi et al. (1991) and Mizota and Iishi (1994) on akermanite solid solutions, (Ca, Sr)$_2$(Mg, Co, Zn, Fe)Si$_2$O$_7$, leading them to conclude that the transition is of second-order. On the other hand, Webb et al. (1992) reported that the IC-N transition in akermanite is associated with a hysteresis effect and a finite unit-cell volume change and thus designated the transition as "weakly first-order". Although we did not observe any significantly macroscopic or microscopic discontinuities across the IC-N transition, our measurements of the intensities of the satellite reflections as a function of pressure indicate the presence of an apparent hysteresis effect associated with the structural transformation, a characteristic of a first-order phase transition that requires some energetic overstepping to initiate the transition.

Since no symmetry change is involved at the IC-N transition in akermanite, there are no restrictions imposed by Landau theory on the order of the transition: it could be of first- or higher order. However, a plot of squared integrated intensities of satellite reflections (I$_s$) against pressure (P) clearly indicates that $I_s^2 \propto (P_{tr}-P)$ (Fig. 8), where P_{tr} is the observed phase transition pressure. Because I$_s$ is generally proportional to the square of the order parameter, Q^2 (Bruce and Cowley 1981), this suggests that the IC-N transition in akermanite is most likely to be tricritical since it implies $Q \propto (P_{tr}-P)^\beta$ with $\beta=1/4$, a characteristic value derived from Landau theory to describe phase transitions that are between continuous and discontinuous (e.g., Salje 1990). The critical phase-transition pressure (P$_c$) estimated from the above relationship is ~ 1.33 GPa.

As mentioned earlier, the mean Ca–O distance in akermanite at ambient conditions is considerably larger than that estimated from the sum of ionic radii (Shannon 1976). This observation suggests that the interlayer Ca cation is too small relative to the square antiprismatic site formed by two five-membered rings. In other words, there is a misfit between the sandwiched Ca cations and

the geometry of the tetrahedral sheets at room pressure; hence, the tendency for tetrahedral sheets to form an adequate interstice for Ca should be responsible for the formation of the N structure. To reduce the mismatch while still maintaining the $P\bar{4}2_1m$ symmetry, the structure responds in two different ways: (1) increasing the degree of the Ca static positional disorder, giving rise to a large and strongly anisotropic displacement ellipsoid, and (2) allowing some sort of distortion of the tetrahedral sheets. Because of the relatively rigid-body character of the $[SiO_4]$ unit, the distortion of the sheets is mainly confined to the libration of the tetrahedron in the (001) plane, resulting in a large amplitude of the tetrahedral librational motion. However, owing to the odd number of tetrahedra in a ring, such a distortion cannot be realized by simple counterrotation of individual tetrahedra within only a single unit-cell of the normal structure; consequently, the incommensurately-modulated structure results from the formation of microdomains. Two microdomain models for the formation of the IC structure in melilites have been proposed so far: one by Van Heurck et al. (1992) based on electron microscopic and diffraction studies on $Ca_2ZnGe_2O_7$ melilite, and the other by Mizota and Iishi (1994) based on heat-capacity measurements on the $(Ca, Sr)_2(Mg, Co, Fe, Zn)Si_2O_7$ solid solutions. Given the entropy associated with the IC-N transition (ΔS), the average domain size in modulated melilites can be estimated from the statistical model of Mizota and Iishi (1994):

$$\Delta S = (R/2n)\ln m,$$

where n and m are the unit cell dimensions (as multiple value of the subcell dimension) of a mean superlattice for the IC phase, and R is the gas constant. For akermanite, the ΔS values reported by Hemingway et al. (1986) and Mizota and Iishi (1994) are 1.9 and 1.6 J/(K mol), respectively; thus the estimated average domain size is between 3×3 and 4×3 subunit cells. A random distribution of domains with 3×4 subcells would then yield a modulation wavelength of 3.46 (in units of the unit cell of the normal structure), which is close to the value of 3.57 observed in this study.

With increasing pressure, the misfit between the interlayer Ca cations and the configuration of the tetrahedral sheets is diminished through the relative rotation and distortion of individual tetrahedra and the differential compression of Ca–O distances, as well as the displacement of Ca along the (110) mirror plane toward the O1 atom. Accompanied with these structural modifications is the great reduction of the positional disorder of Ca and the librational amplitude of the $[SiO_4]$ unit, which in turn results in the decrease in intensities of satellite reflections and thus the amplitude of modulation. Figure 9 illustrates such relationships: the satellite intensities vary linearly with the isotropic displacement parameter of Ca and the librational amplitude of the $[SiO_4]$ tetrahedron. Therefore, the changes in the Ca positional disorder and the librational amplitude of the $[SiO_4]$ group can be regarded as the primary driving force for the IC-N
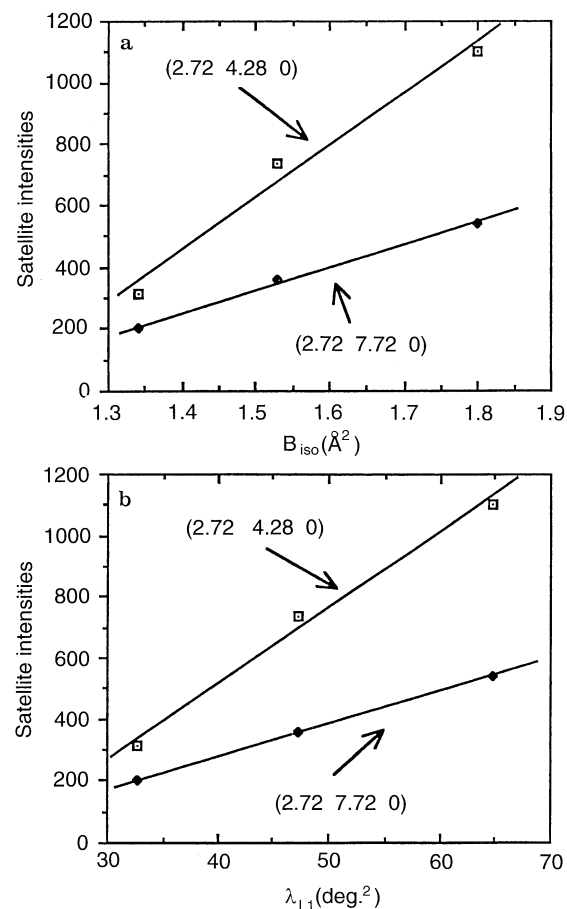

Fig. 9 a Satellite intensities vs. the isotropic displacement parameter (B_{iso}) of Ca and **b** satellite intensities vs. the largest librational eigenvalue (λ_{L1}) of the $[SiO_4]$ tetrahedron

transformation. In fact, these two factors are linearly coupled, as shown in Figure 9. At a sufficiently high pressure ($\sim$1.33 GPa in this study) the mismatch between Ca cations and tetrahedral sheets is eliminated; hence, the microdomains in the modulated structure are minimized and a high-pressure normal structure occurs. The hysteresis effect observed during the release of pressure may result from the formation of microdomains from the normal structure, which would require some extra energy to overcome strain induced by the misfit between Ca cations and tetrahedral sheets.

The above discussion suggests that the mechanism of the IC-N transition induced by increasing pressure is different from that induced by increasing temperature. The normal structure at high temperature has been considered as a consequence of the dynamic averaging of microdomains in the modulated structure (Van Heurck et al. 1992). The dynamic nature of the normal phase at high temperature has been directly confirmed by Mössbauer spectroscopic measurements of Fe-akermanite (Seifert et al. 1987). At room temperature the IC phase exhibits two distinct environments containing (Mg+Fe); the difference between these two sites become gradually less pronounced with increasing temper-

ature and indistinguishable above the IC-N transition temperature. Further evidence for the dynamic averaging of microdomains resulting in the normal phase comes from the ^{29}Si MAS NMR study by Merwin et al. (1989). Spectra on the modulated akermanite at 298 K consist of 3 or 5 peaks, indicating the existence of 3 to 5 nonequivalent Si sites in the structure; at elevated temperatures these peaks merge into a single, sharp peak at 380 K, characteristic of the normal structure.

References

Armbruster TF, Röthlisberger F, Serfert F (1990) Layer topology, stacking variation and site distortion in melilite related compounds in the system CaO–ZnO–GeO$_2$–SiO$_2$. Am Mineral 75:847–858

Becker PJ, Coppens P (1975) Extinction within the limit of validity of the Darwin transfer equations: III. Non-spherical crystals and anisotropy of extinction. Acta Crystallogr A31:417–425

Brown ID (1981) The bond-valence method: An empirical approach to chemical structure and bonding. In: O'Keeffe M, Navrotsky A (ed) Structure and Bonding in Crystals. Academic Press, New York

Brown NE, Ross CR II, Webb SL (1994) Atomic displacements in the normal-incommensurate phase transition in Co-akermanite (Ca$_2$CoSi$_2$O$_7$). Phys Chem Minerals 21:469–480

Bruce AD, Cowley RA (1981) Structural Phase Transitions. Taylor and Francis, London

Finger LW, King H (1978) A revised method of operation of the single-crystal diamond cell and refinement of the structure of NaCl at 32 kbar. Am Mineral 63:337–342

Finger LW, Prince E (1975) A system of FORTRAN IV computer programs for crystal structure computations. National Bureau of Standards Technology Note 854

Hagiya K, Ohmasa M, Iishi K (1993) The modulated structure of synthetic Co-akermanite, Ca$_2$CoSi$_2$O$_7$. Acta Crystallogr B49:172–179

Hazen RM, Finger LW (1977) Crystal structure and compositional variation of Angra dos Reis fassaite. Earth Planet Sci Lett 35:357–362

Hazen RM, Finger LW (1978a) The crystal structures and compressibilities of layer minerals at high pressure. II. Phlogopite and chlorite. Am Mineral 63:293–296

Hazen RM, Finger LW (1978b) Crystal structures and compressibilities of pyrope and grossular to 60 kbar. Am Mineral 63:297–303

Hazen RM, Finger LW (1982) Comparative Crystal Chemistry. Wiley, New York

Hemingway BS, Evans HT, Nord GL, Haselton HT, Robie RA, McGee JJ (1986) Akermanite: Phase transitions in heat capacity and thermal expansion, and revised thermodynamic data. Can Mineral 24:425–434

Ibers JA, Hamilton WC (1974) International tables for X-ray crystallography. Vol. IV, 336 p. Kynoch, Birmingham, U.K.

Iishi K, Fujimoto K, Fujino K (1989) Single crystal growth of akermanites Ca$_2$(Mg$_{1-x}$Co$_x$)Si$_2$O$_7$ with modulated structure. N Jb Mineral Monatsh 1989:219–226

Iishi K, Fujino K, Furukawa Y (1990) Electron microscopy studies of akermanites (Ca$_{1-x}$Sr$_x$)$_2$CoSi$_2$O$_7$ with modulated structure. Phys Chem Minerals 17:467–471

Iishi K, Mizota T, Fujino K, Furukawa Y (1991) Heat capacity anomalies at incommensurate-normal transition of akermanite solid solution (Ca, Sr)$_2$(Mg, Co, Zn, Fe)Si$_2$O$_7$. Phys Chem Minerals 17:720–725

Iishi K, Hagiya K, Ohmasa M (1994) Circular diffuse scattering of akermanite studied by the optical diffraction method. Phys Chem Minerals 21:6–11

Kimata M, Ii N (1981) The crystal structure of synthetic akermanite, Ca$_2$MgSi$_2$O$_7$. N Jb Mineral Monatsh 1981:1–10

Kimata M, Ohashi H (1982) The crystal structure of synthetic gugiaite, Ca$_2$BeSi$_2$O$_7$. N Jb Mineral Abh 143:210–222

King HE, Finger LW (1979) Diffracted beam crystal centering and its application to high-pressure crystallography. J Appl Crystallogr 12:374–378

Lehmann MS, Larsen FK (1974) A method for location of the peaks in step-scan-measured Bragg reflexions. Acta Crystallogr A30:580–584

Levien L, Prewitt CT (1981) High-pressure structural study of diopside. Am Mineral 66:315–323

Li Z, Chan S-K, Ghose S (1990) Elastic properties of the incommensurate phase of akermanite, Ca$_2$MgSi$_2$O$_7$. Phys Chem Minerals 17:462–466

Merwin LH, Sebald A, Seifert F (1989) The incommensurate-commensurate phase transition in akermanite, Ca$_2$MgSi$_2$O$_7$, observed by in-situ ^{29}Si MAS NMR spectroscopy. Phys Chem Minerals 16:752–756

Mizota T, Iishi K (1994) Heat capacity measurements around incommensurate-normal phase transition of synthetic akermanite solid solutions and the transition entropies. Netsu Sokutei 21:12–19

Robinson K, Gibbs GV, Ribbe PH (1971) Quadratic elongation: A quantitative measure of distortion in coordination polyhedra. Science 172:567–570

Röthlisberger F (1989) Zusammehang zwischen Chemismus, Stabilität und struktureller Variation der Melilite. Thesis, University of Bayreuth

Röthlisberger F, Seifert F, Czank M (1990) Chemical control of the commensurate-incommensurate phase transition in synthetic melilites. Eur J Mineral 2:585–594

Salje EKH (1990) Phse Transitions in Ferroelastic and co-elastic crystals. Cambridge University Press, New York

Seifert F, Röthlisberger F (1993) Macroscopic and structural changes at the incommensurate-normal phase transition in melilites. Mineral Petrol 48:179–192

Seifert F, Czank M, Simons B, Schmahl W (1987) A commensurate-incommensurate phase transition in iron-bearing akermanites. Phys Chem Minerals 14:26–35

Shannon RD (1976) Revised effective ionic radii and systematic studies of interatomic distances in halides and chalcogenides. Acta Crystallogr A32:751–767

Shannon RD, Iishi K, Allik TH, Rossman GR, Liebertz J (1992) Dielectric constants of BaO and melilites and the oxide additivity rule. Eur J Mineral 4:1241–1249

Sharma SK, Yoder HS Jr., Matson DW (1988) Raman study of some melilites in crystalline and glass states. Geochim Cosmochim Acta 52:1961–1967

Swainson IP, Dove MT, Schmahl WW, Putnis A (1992) Neutron powder diffraction study of the akermanite-gehlenite solid solution series. Phys Chem Minerals 19:185–195

Tamura T, Yoshiasa A, Iishi K, Takeno S, Maeda H, Emura S, Koto K (1996) Local structure of (Ca, Sr)$_2$(Mg, Co, Zn)Si$_2$O$_7$ melilite solid-solution with modulation structure. Phys Chem Minerals 23:81–88

Trueblood KN (1978) Analysis of molecular motion with allovance for intermolecular torsion. Acta Crystallogr A34:950–954

Van Heurck C, Van Tendeloo G, Amelinckx S (1992) The modulated structure in the melilite Ca$_2$ZnSi$_2$O$_7$. Phys Chem Minerals 18:441–452

Webb SL, Ross CR, Liebertz J (1992) Thermal expansion and spontaneous strain associated with the normal-incommensurate phase transition in melilites. Phys Chem Minerals 18:522–525